Composite Structures 135 (2016) 61–73

Contents lists available at ScienceDirect

Composite Structures

journal homepage: www.elsevier.com/locate/compstruct

Matrix failure in composite laminates under tensile loading

Nayeem Tawqir Chowdhury [a,*], John Wang [b], Wing Kong Chiu [a], Wenyi Yan [a]

[a] Department of Mechanical and Aerospace Engineering, Monash University, Clayton, VIC 3800, Australia
[b] Aerospace Division, Defence Science and Technology Organisation, 506 Lorimer St., Fishermans Bend, VIC 3207, Australia

ARTICLE INFO

Article history:
Available online 25 September 2015

Keywords:
Matrix failure
Composites
Biaxial tension
Truncation
Failure envelope

ABSTRACT

The failure envelope of the matrix in composite laminates under tensile loads has not received much attention in literature. There are very little to no experimental results to show a suitable failure envelope for this constituent found in composites. With increasing popularity in the use of micromechanical analysis to predict progressive damage in composite structures, it is important that matrix behaviour under tension is modelled correctly. In this paper, the authors present and test a new biaxial specimen design to investigate tensile matrix failure in composite structures. Through the use of micromechanical analysis, the authors developed a method in which the matrix stresses at failure can be extracted. Comparing to the existing off-axis test, it was shown that the presented specimen design and test methodology can improve the accuracy of the obtained matrix failure stresses, i.e., the matrix failure envelope for EP280 resin. Additionally, the results indicate that matrix failure takes place earlier than that predicted by von-Mises failure criterion and that the 1st Stress Invariant criterion can better predict matrix failure under tensile loading.

1. Introduction

Fibre reinforced polymer materials are increasingly being used due to their high strength to weight ratio and high fatigue resistance. Despite this, there are still many unanswered questions as to the materials' failure characteristics as composites can be characterised by fibre, matrix and interfacial failure [1].

It is computationally prohibitive to model a composite structure with each strand of fibre despite being able to extract the stress and strain states of the fibre, matrix and interface separately. One method that has greatly assisted in simplifying this analysis is Classical Laminate Theory (CLT) [2]. This theory combines the properties of the fibre and the matrix through an averaging approach to form a new homogenous material called a lamina. CLT is widely used by researchers in the field and given its simplicity it does a good job at modelling the stiffness of a laminate including linear load behaviour up to the point of failure. One improvement that can be made to this theory would be the ability to separately examine the fibre and the matrix. This can be done using micromechanical analysis.

Micromechanical analysis can be used to separate the stress and strain in the matrix and fibre from a representative volume element (RVE). These can then be used to predict matrix or fibre failure in a structural analysis. One popular analysis method that uses micromechanical analysis is Multicontinuum Theory (MCT) [3,4]. MCT predicts failure at the fibre and matrix level by obtaining the volume averaged stress states in the fibre and the matrix. Here, matrix failure is assumed to be influenced by all six of the matrix average stress components in a 3D analysis, whilst a quadratic function is used to find the average stress of the fibre [3]. This particular theory greatly assists with understanding matrix failure and fibre failure in a composite, especially when it comes to progressive damage models [5–7]. However, the assumption of averaging the overall stresses in the individual constituents can be improved on. An analysis method that does this is the amplification technique [8–10]. Unlike MCT, where the stresses in each constituent are averaged, the amplification technique calculates the principal stresses and strains at several locations to identify a critical location. Using this separation technique allows the fibre and matrix failure to be examined in detail.

Fibre failure has been quite extensively researched in the field of composites, whilst at a micromechanical level, matrix failure has not received the same amount of attention. Matrix failure is typically known to take place well before the fibre in matrix dominated load cases and can be characterised by three main modes: tension, compression and shear failure. Some authors have proposed these modes of failure to be characterised by dilatational failure and distortional failure [8,9,11]. In this paper the authors focus on tensile matrix failure in composites.

* Corresponding author.
E-mail address: nayeem.chowdhury@monash.edu (N.T. Chowdhury).

http://dx.doi.org/10.1016/j.compstruct.2015.09.022
0263-8223/

Matrix failure under tension loading has received some attention in literature where some have performed a range of off-axis tests on uniaxial composites [12]. However improvements to this method can be made. For example testing a 45° off axis specimen can only give the user one data point for failure, in order to obtain several more failure points, the fibre angle should be varied. However, as more angles are tested, the difference between them is minimal and subject to manufacturing errors. For example: two specimens; one with 45° fibre orientation and the other with 47° fibre orientation. Along with this others have stated how the off-axis tensile tests suffer from premature failure due to the way the specimens are constrained when being loaded [13–15]. This raises the question of whether the measured data from off-axis tests are accurate. One method in which these tests can be improved is through performing biaxial tension–tension tests. This would mean that for a given fibre orientation, the load ratios can be varied to obtain more than one data point for failure. Biaxial test results and specimen designs have been presented in literature [16–18]. The findings from these can be used to create a new test specifically examining matrix failure.

In the past, experimental data for isotropic materials has been used to propose various failure criteria. Some of which include maximum stress theory, von-Mises, Drucker–Prager, and Mohr–Coulomb. The availability of data has allowed certain models to be refined. For example, maximum stress theory, Drucker–Prager, and Mohr–Coulomb all suggest a truncation in the tensile quadrant of a principal stress based failure envelope [8,9]. However the lack of experimental data to explain the onset of failure (matrix failure) in composites under tensile stress states has hindered research in composites. Through the use of micromechanical analysis and by designing and testing a biaxial fibre reinforced specimen, this void of information can start to be populated.

In this paper the authors aim to design and test a fibre reinforced biaxial specimen by overcoming some of the difficulties presented in literature with performing such tests [19]. The authors use a modified version of a specimen design previously presented to test isotropic materials under biaxial loads [20,21]. Uniaxial off-axis tests are also performed using the same material to highlight the significance of performing biaxial tests. The study is concluded by comparing against a third set of experiments performed on a biaxial specimen made of the matrix material called EP280 [22].

2. Matrix failure in CFRP under biaxial tensile loading

The main objective of this paper is to establish the tensile failure envelope for the matrix. In order to do this the authors have modified an existing biaxial specimen design created for testing isotropic materials [20,21,23]. The specimen design was found to achieve a 98% higher stress state at the centre gauge region compared to anywhere else in the specimen allowing for a successful biaxial test [23]. The biaxial tests were performed on a machine designed by the authors which uses two computer controlled actuators placed on a set of linear bearings which allows the specimen to deform in a uniform manner which is important in such tests [21].

2.1. Experiment methodology

The material being tests is called EP 280 Prepreg which has a ply thickness of 0.25 mm. The authors use two plies within the centre gauge region and a further 10 plies to form the surrounding geometry. It is important to have ply drop-offs at each layer in order to avoid introducing significant out of plane peal stresses. The final specimen design is shown in Fig. 1. The diameter of the holes in each ply can be chosen so that a smooth conical transition can be achieved. If a different thickness material is used or different centre gauge thickness is requires, then through the use of Eqs. (1) and (2); the required punch diameters can be calculated. The authors used existing imperial and metric sized punches to produce these holes, thus the uneven reduction in hole diameters. This uneven transition does not affect the overall specimen geometry as the external surfaces are pressed against two aluminium moulds to ensure that the geometry is maintained to the same dimensions as that used by the authors previously [20,21,23].

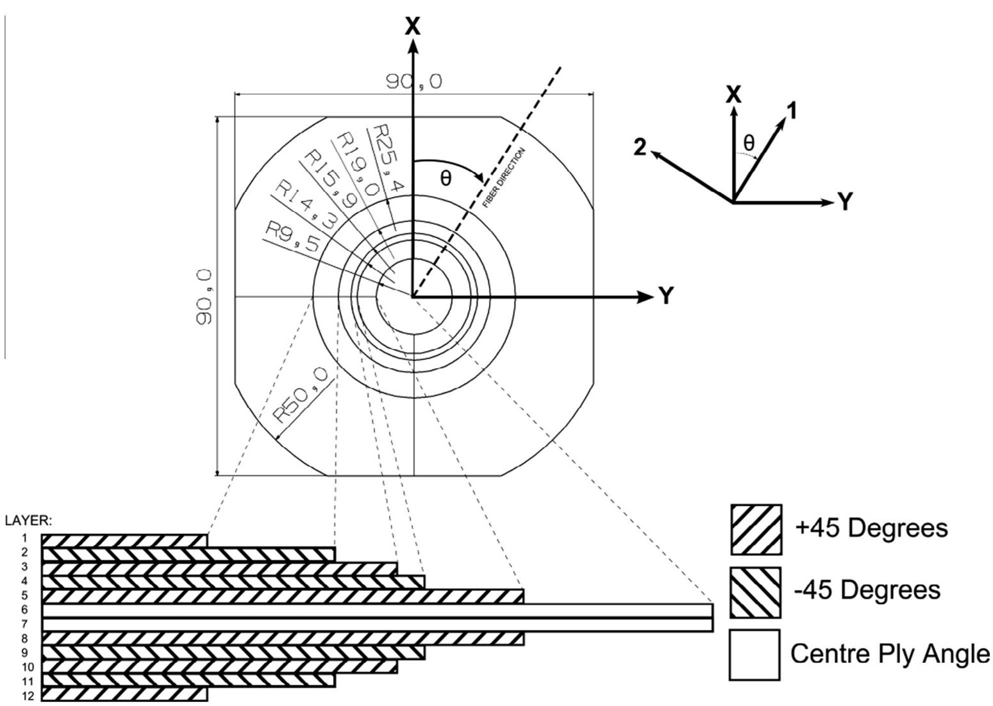

Fig. 1. Specimen design (top view) with lamina orientation and ply drop offs (0.25 mm ply thickness).

Focus on preparing each layer of the laminate is required when manufacturing the biaxial specimen. Fig. 1 shows the layering of several plies of prepreg carbon, where layers 6 and 7 make up the gauge region. As matrix failure is being examined in this paper, the centre two gauge regions have fibres aligned in the same direction to promote this mode of failure (for example, 2 layers of +30° fibres placed in the centre gauge region). Fig. 2a shows the general manufacturing process. Eqs. (1) and (2) summarises the relationship found by the authors in a previous investigation where a parametric study was performed examining the optimum thickness of the gauge region such that failure does not occur at the clamps. Along with choosing an appropriate transition radius so that premature failure at this location does not take place [23]. The equations were proposed as a guide to researchers aiming to come up with their own flat pate biaxial specimen design.

$$\frac{\text{Gage thickness}}{\text{Thickness at clamps}} \leqslant 0.1 \tag{1}$$

$$\frac{\text{Transition Radius}}{\text{Gage Diameter}} \geqslant 1 \tag{2}$$

The authors suggest the use of alternating ±45° fibres for all layers outside the gauge region. The specimens were cured in an autoclave for 60 min at 120 °C with a ramp up rate of 2 °C/min at 100 kPa [22]. Fig. 2b shows the final specimen used for testing.

2.2. Experimental results

Biaxial tensile tests have not been published in great detail in literature due to the difficulties associated in performing such tests [19]. The specimen design to some extent is simpler to test compared with an isotropic material as the fibre directions can be chosen to promote matrix failure.

One thing to note is that this specimen will continue to carry load after the gauge region has failed as the surrounding reinforcing layers remain intact. This can create issues when detecting failure as preliminary tests demonstrated that the critical point at which the matrix fails cannot be detected easily on the load–displacement curve. This issue is overcome using a FLIRE thermal imaging camera (Fig. 3). The matrix failure causes a momentary spike in temperature which is picked up by the camera. The cameras acquisition rate was set to 6 frames per seconds which was found to be adequate for capturing the initial failure. This is due to the fact that although failure occurs very suddenly, the temperature spike picked up by the thermal camera takes a few seconds to fully dissipate. The load at failure was then recorded for each of the tests.

Six different fibre orientations are tested: 45°, 40°, 30°, 20°, 10°, and 0°. Several tests for each fibre direction are performed with different loading ratios. Forces in the x and y direction are listed in Table 1 for the different tests performed.

2.3. Finite element analysis

Current experimental techniques are not able to distinguish stress or strain states on the matrix and fibre independently, and usually stop at the laminate (global) level. Obtaining stress and strain data for the matrix requires post processing of the experimental results. This is done through finite element analysis for this study. The technique separates the global stresses in the laminate to find individual stresses on the fibre and the matrix.

An ideal method in which the failure stresses on the matrix can be obtained is to create a large analysis with each individual strand of fibre modelled, surrounded by the matrix for the entire test specimen. However using to days computing power; this is almost impossible to perform in a reasonable amount of time. The next best alternative is to extract the stress and strain state at a critical location in the global (macro) model, then impose these as boundary conditions to a unit cell. The unit cell is a representative volume element (RVE) of the fibre and the matrix that can be found at the micro scale. This method has started to gain popularity and is considered to be an acceptable means of establishing the micromechanical stress state in the fibre and the matrix [8–10,24]. In order to account for the random arrangement of fibres within a lamina; the process performed on a square unit cell is repeated for a diamond, and hexagonal fibre configuration. The procedure is summarised in Fig. 4.

The first stage in this approach is to obtain the stress and strain state in a global macromechanical model. Strain gauges in several experiments were used to check that the FE model gave a good prediction of this. However, a strain gauge cannot solely be used for this stage as we are after both in-plane and out of plane stress states. Thus FEA aids in this process.

The properties of the lamina were experimentally determined using ASTM D3039 [25] and ASTM D5379 [26]. The material properties for EP280 Prepreg are listed in Table 2. The rule of mixtures is used to calculate the individual properties of the fibre and matrix [27]. For simplicity both the fibre and matrix are considered to be isotropic in nature. The material was supplied with a 50% fibre volume fraction. Micromechanical analysis using RVEs was used to check the properties in Table 3 against those listed in Table 2. It is found that the results closely match with a difference of less than 10%, thus Table 3 properties were adopted as the isotropic properties of the fibre and the matrix.

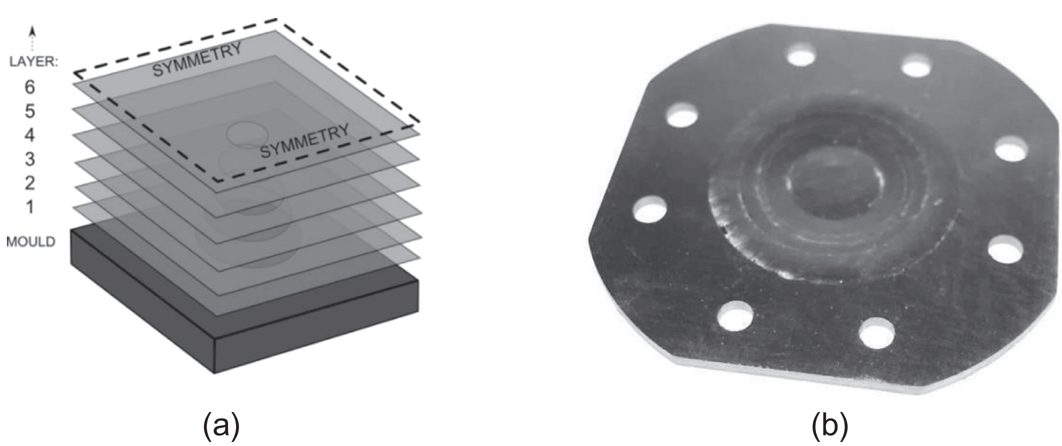

Fig. 2. (a) Layers 1–6 out of 12 layers of Prepreg carbon with varying hole diameters to form a composite specimen. (b) Final cured and machined specimen.

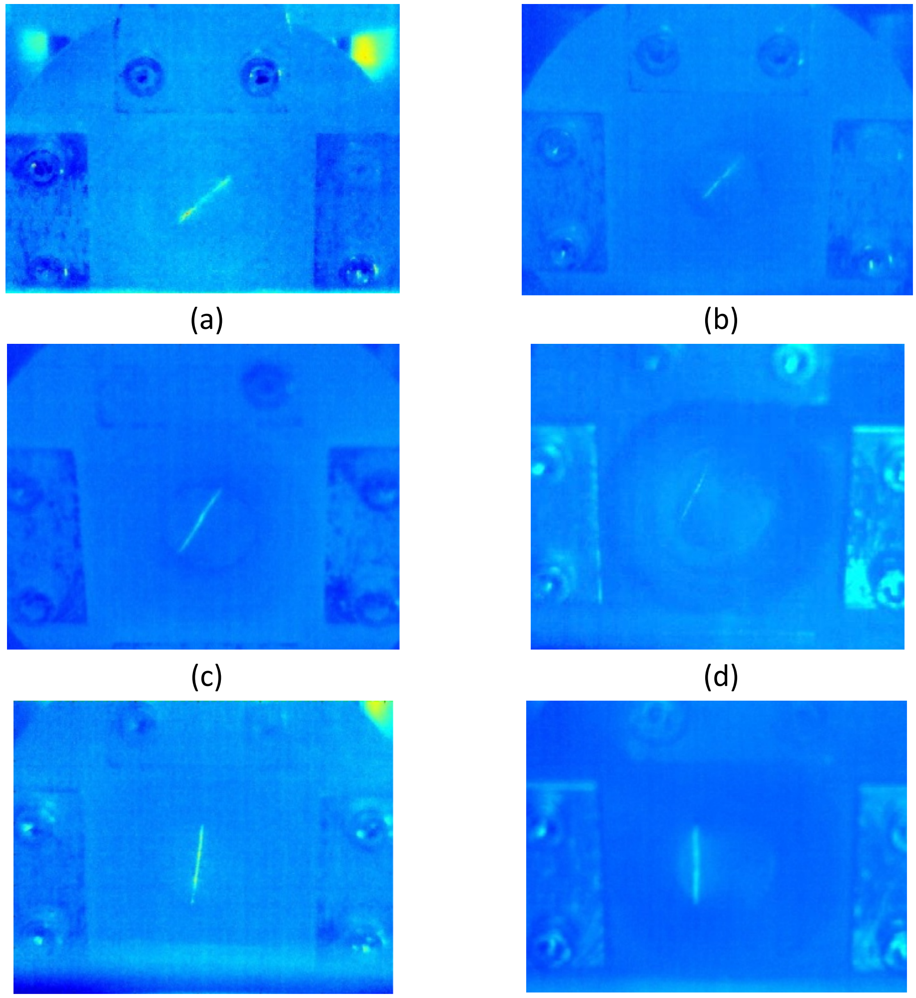

Fig. 3. Thermal camera showing point of failure for a: (a) 45° specimen, (b) 40° specimen, (c) 30° specimen, (d) 20° specimen, (e) 10° specimen, (f) 0° specimen.

Table 1
Experimental forces at failure for biaxial FR tests.

TEST	Fibre angle (°)	Failure force in the *X* direction (N)	Failure force in the *Y* direction (N)	Load ratio	TEST	Fibre angle (°)	Failure force in the *X* direction (N)	Failure force in the *Y* direction (N)	Load ratio
1	45	5932	10,218	0.6	14	20	10,087	10,223	1.0
2	45	7882	8716	0.9	15	20	2626	5270	0.5
3	45	3087	10,844	0.3	16	20	2906	5937	0.5
4	45	7041	6694	1.1	17	20	5840	7906	0.7
5	45	7017	8999	0.8	18	10	5714	5498	1.0
6	45	6454	6088	1.1	19	10	7656	6724	1.1
7	40	5726	7118	0.8	20	10	9584	8526	1.1
8	40	8410	7285	1.2	21	10	11,511	9602	1.2
9	30	671	5149	0.1	22	0	6021	7209	0.8
10	30	6985	7451	0.9	23	0	1914	5255	0.4
11	20	7753	9072	0.9	24	0	9318	8390	1.1
12	20	10,589	10,980	1.0	25	0	2710	6755	0.4
13	20	3004	6830	0.4	26	0	1160	4680	0.2

The finite element analysis package: FEMAP v10.0.2 was used to model the specimen [28]. Each ply is modelled as a separate section using 3D solid hexahedral elements. One element is used through the thickness of each ply. The coincident nodes between layers are tied together assuming a perfectly bonded surface. Each ply is assigned a separate material property depending on its fibre orientation. Using the properties listed in Table 2, the stiffness matrix for the material is determined and rotated about the *z*-axis using the bond transformation matrix [29]. This ensures that the global properties are oriented in the local axis for the analysis. The 1, 2 and 3 directions represent the fibre, transverse and out of plane directions respectively. Six out of the twelve layers are modelled to be computationally efficient and a symmetry constraint is applied to the bottom surface of layer six shown in Fig. 1.

End effects from the clamps and boundary conditions applied to the specimen are important to consider in both experimental setup

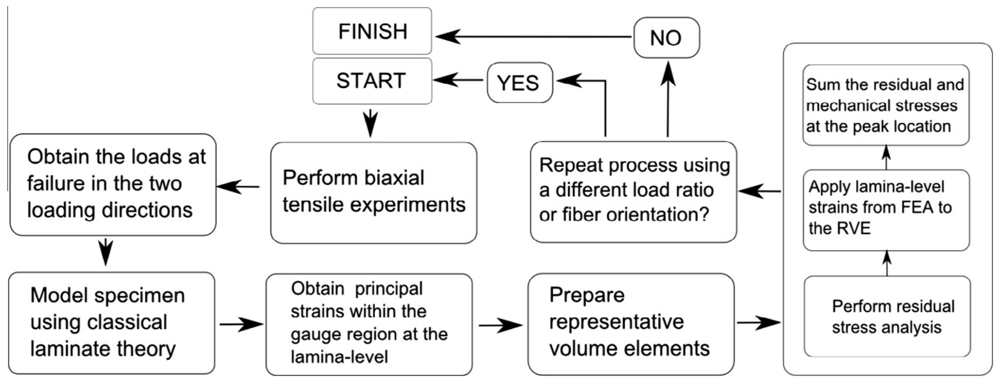

Fig. 4. Methodology used to post process experimental results.

Table 2
Material properties for EP 280 Prepreg.

Property	
$E11$	131 GPa
$E22$	6.20 GPa
$E33$	6.20 GPa
$v12$	0.28
$v23$	0.40
$v13$	0.28
$G12$	4.73 GPa
$G23$	1.44 GPa
$G13$	4.73 GPa

Table 3
Calculated properties for the fibre and matrix.

Property	Fibre	Matrix
E	259 GPa	3.140 GPa
V	0.30	0.30

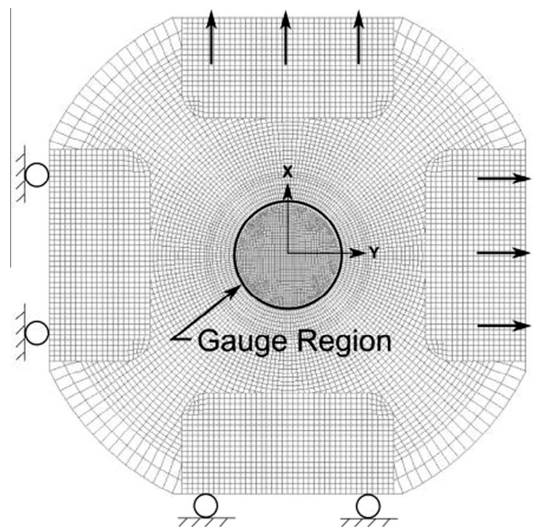

Fig. 5. Meshed specimen with identification of gauge region, tab locations and boundary conditions.

and in the FE model [14,30]. The specimen design in this case is somewhat advantageous as the gauge region is quite far from any constraints thus assisting in the way in which the loads are applied in the FE model [31]. The authors apply loads as surface traction forces on tabbed surfaces which are perfectly bonded to the surface of the specimen (Fig. 5). This is to closely model the way in which loads are transferred from the clamps on the test machine to the specimen. Note that the contact surfaces of the clamps have a coarse grit paper applied to distribute the load to the surface of the specimen as opposed to directly on the bolt holes. From a previous study performed by the authors it is found that the gauge region of the specimen experiences a homogeneous stress distribution [20,21]. For this reason the strain state on the centre node (the origin of the Cartesian axis shown in Fig. 5) is obtained for each analysis.

Fig. 6 shows the stress contour plot for layers 1–6 of the biaxial specimen. Note that the first FEA result was compared against experimental results using a delta strain gauge rosette. A difference of less than 10% was achieved, thus the values in Table 2 were used to analyse the specimen. As can be seen in Fig. 6, despite the lamina being highly orthotropic in nature, through the use of ±45° surrounding layers; the centre two plies (layer 6 and 7) experience a peak stress concentration in the gauge region. This is desired in order to satisfy the conditions of a successful biaxial test [19–21].

All the experiments were tested for buckling and geometric nonlinear tendencies in FEMAP. None of the specimens were found to have suffered from buckling which can potentially take place within the gauge region at very high load ratios when the Poisson's effect overcomes the slight tension in the other axis resulting in a net compressive stress state. The geometric nonlinear analysis showed the strain results to vary by less than 1% and thus geometric linear analysis was considered to be sufficient for modelling purposes. Once analysis of the global model was completed, the strains in the centre gauge region were used as inputs for the micromechanical stage of the analysis.

An important consideration when performing RVE analysis is to ensure that periodic boundary conditions are maintained such that if several of the same unit cells are to be stacked next to each other; there should be no gaps between them [8,9]. Maintaining periodic boundary conditions while applying normal and shear strains to a single RVE is difficult to do. To overcome this, the authors modelled two unit cells; one for normal strains and the other for shear strains. The results are then superimposed according to Eq. (3).

$$\begin{Bmatrix} S_{11}^{s} \\ S_{22}^{s} \\ S_{33}^{s} \\ S_{12}^{s} \\ S_{23}^{s} \\ S_{13}^{s} \end{Bmatrix} = \begin{Bmatrix} S_{11}^{RVE1} \\ S_{22}^{RVE1} \\ S_{33}^{RVE1} \\ S_{12}^{RVE1} \\ S_{23}^{RVE1} \\ S_{13}^{RVE1} \end{Bmatrix} + \begin{Bmatrix} S_{11}^{RVE2} \\ S_{22}^{RVE2} \\ S_{33}^{RVE2} \\ S_{12}^{RVE2} \\ S_{23}^{RVE2} \\ S_{13}^{RVE2} \end{Bmatrix} \tag{3}$$

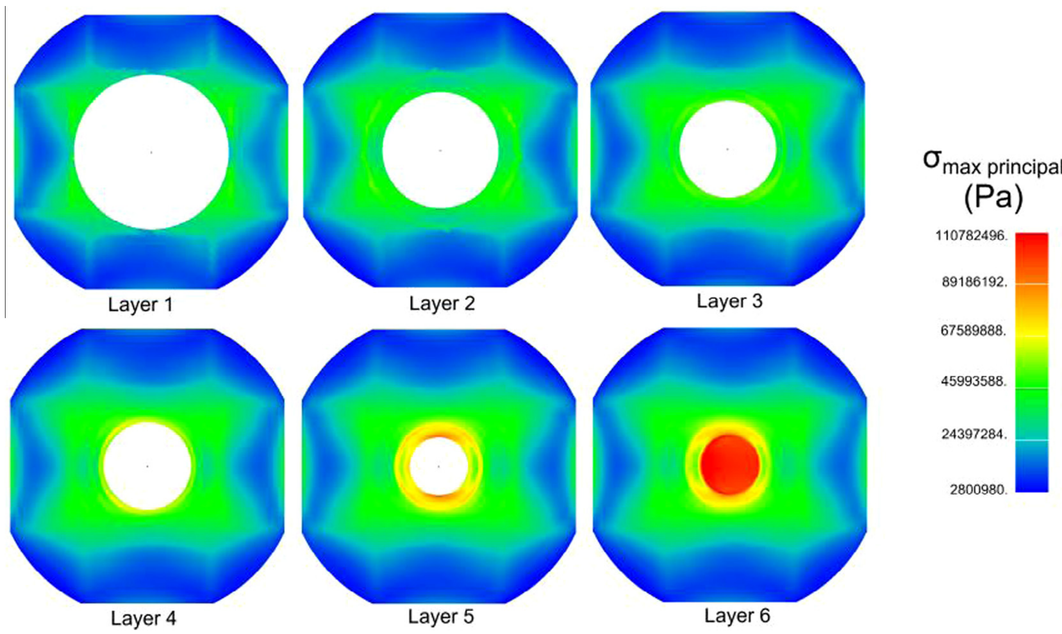

Fig. 6. Stress contour plot for layers 1–6 for test 1 using a 45° specimen (Table 1).

where:

Superscript 'RVE1' represent the stresses obtained from representative volume element 1 involving the normal loads (Fig. 7a).

Superscript 'RVE2' represent the stresses obtained from representative volume element 2 involving the in-plane shear loads (Fig. 7b).

Superscript 'S' represent the stresses obtained from RVE1 and RVE2 after superimposing the results.

In the RVEs all the sides must remain flat and parallel to their opposing face. In the first RVE (Fig. 7a), three of the six faces are constrained using symmetry constrains that allow the face to expand or contract within its plane but restricts movements perpendicular to its face. The other three faces have strains applied on them using the values obtained from the macromechanical FE model. These include the strains along the fibre, perpendicular to the fibre and in the out of plane directions. In the second RVE (Fig. 7b), the out of plane faces are fixed in the '3' direction whilst displacements are applied parallel to the 1, and 2 directions simulating a shearing load.

The location of the maximum principal stresses differs depending on the type of fibre configuration used (square, diamond, vertical hexagonal, or horizontal hexagonal); this is shown in Fig. 8. When the stresses are obtained from the model they must all be probed from the one location which is termed the critical location. Thus state variables (STATEV) in ABAQUS 6.13 were used to obtain a contour plot (Fig. 9) of the 1st Stress Invariant [32]. This allowed the critical location to be identified and the values of σ_{11}, σ_{22} and σ_{33} to be probed in the regions shown in red. Reasons why the 1st Stress Invariant was chosen will be discussed in Section 5.

The next process is to calculate the principal stresses at failure for the matrix. From the finite element model it is found that the two out of plane shear stress values were very low and thus

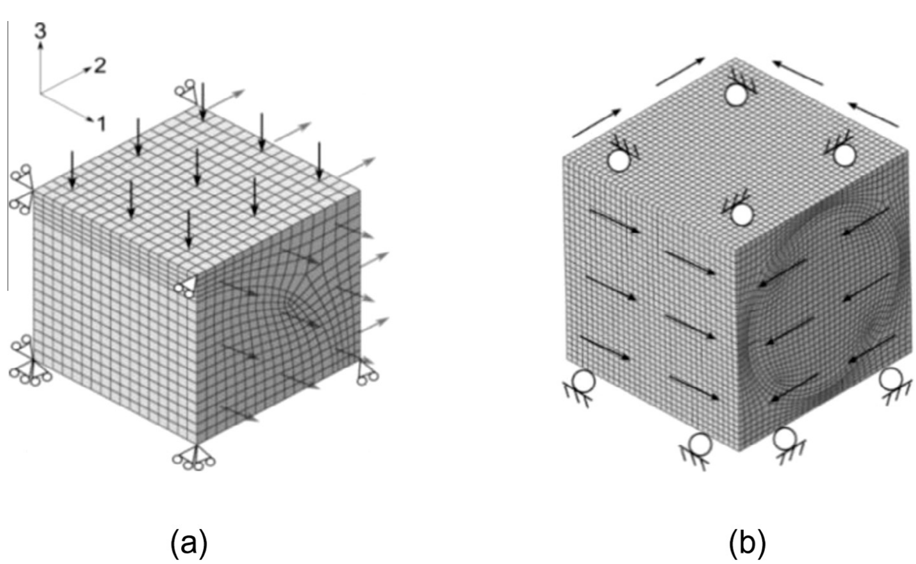

Fig. 7. Boundary conditions applied to a square fibre configuration RVE. (a) Example of normal strains applied to the RVE, (b) example of shear strains applied to the RVE.

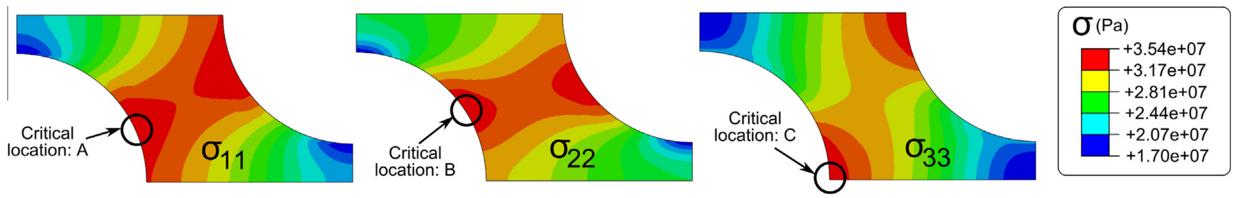

Fig. 8. Normal stress plot demonstrating different critical stress locations on the matrix (horizontal hexagonal RVE).

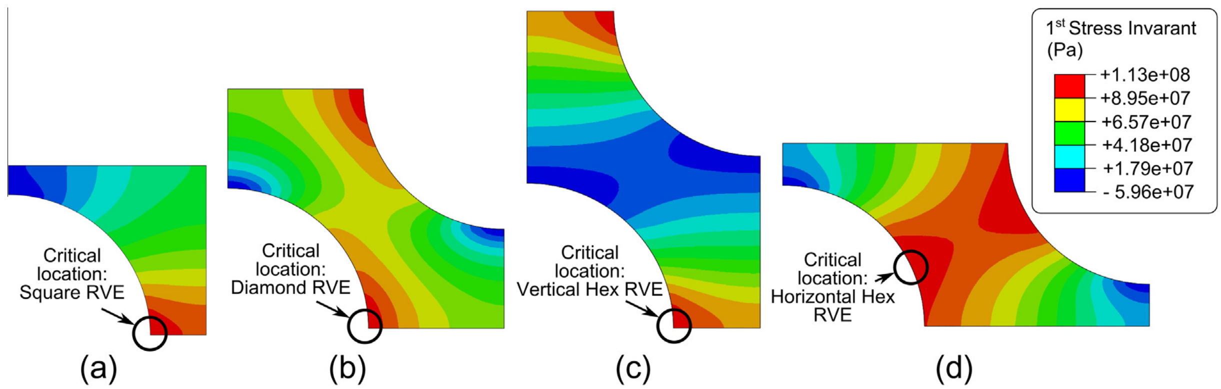

Fig. 9. Plot of the 1st Stress Invariant on the matrix for a: (a) square configuration, (b) diamond configuration, (c) vertical hexagonal configuration, (d) horizontal hexagonal configuration.

ignored in the superimposing method. The remainder stresses were used to calculate the principal stresses according to Mohr's Circle in three dimensions.

The final stage of the analysis is the consideration of hygrothermal stresses. The importance of incorporating thermal residual stress analysis is debated in literature when it comes to composites [33]. Some existing failure criterions such as Onset Theory have thermal residual stress parameters within their model. These stresses are recommended to be added on to the mechanical strains after performing micromechanical analysis [8]. Whilst others have argued that the residual stresses tend to relax over time [34,35]. For this investigation the thermal residual stresses are considered to be offset by the absorption of moisture by the material between the time of cure and testing. This was investigated by the authors in a previous study [36]. Regardless of any assumptions made about hygrothermal stresses, the trends presented in this paper are believed not to change.

2.4. Processed results

The final processed results listing the principal stresses at failure for the matrix obtained under biaxial testing are shown in Table 4.

3. Matrix failure in CFRP under uniaxial Off-axis tension

Uniaxial off-axis tension tests have been performed by several authors in the past [12,14,15]. A similar test methodology was adopted to explore the failure envelope for the material used in this investigation (EP280 Prepreg). Steep fibre angles are avoided in this study as they have been reported to exhibit a distortional mode of failure [12] which is not of interest in this paper. As the specimens are made up of the same material used in the biaxial test, it is expected a similar observation will be seen. Any differences in results will highlight the advantage of performing actual biaxial tests as opposed to off-axis tests to observe matrix failure.

3.1. Experiment methodology

ASTM D3039 is used for the specimen design [25]. Fig. 10 shows the overall specimen dimensions. The use of oblique tabs has been proposed by several authors to minimising the shear stress that is introduced in such tests due to the fibre layout [14,15,19]. The tabs are also considered to minimise the stress concentration that takes place at the ends of the specimen during clamping. However the authors did not have success in their use as failure originated at the tip of the oblique tab. Thus square tabbed specimens (which is suggested in the ASTM D3039) were used. Fig. 11, shows the pictures of several off-axis specimens after failure. The 20° and 10° angles were not tested as these are known to fail due to shear [12,37], whilst the 0° fibre angle is a characterised by fibre failure. These two modes of failure are not of interest in this paper.

3.2. Processed results

The processing of the experimental results is the same as that discussed for the biaxial specimens in Section 2.3 and Fig. 4. The main difference is that the macro model of the specimen is modelled according to Fig. 10. Micromechanical analysis is also performed using the same four fibre configurations. The processed results for the matrix are shown in Table 5.

4. Failure in a neat resin under biaxial tensile loading

The final specimen being discussed in this paper is the biaxial neat resin specimen. The neat resin specimen uses the same resin found in the carbon prepreg specimens. The purpose of using such a material is to see if there is a relationship between the tests on a specimen with and without the presence of fibres.

4.1. Experiment methodology

The specimen design presented by the authors in previous studies [20,21] was used to the perform biaxial tension–tension tests.

Table 4
Principal stresses obtained from experiments for biaxial FR tests and their standard deviation based on four fibre configurations (square, diamond, vertical hex and horizontal hex).

Test N°	Fibre angle (°)	σ_1 (MPa)	σ_2 (MPa)	σ_3 (MPa)	Standard deviation σ_1 (MPa)	Standard deviation σ_2 (MPa)	Standard deviation σ_3 (MPa)
1	45	137.65	32.61	4.60	29.92	13.72	9.20
2	45	95.58	50.92	33.62	25.68	12.00	14.08
3	45	178.02	28.10	−55.32	35.45	11.87	10.98
4	45	76.54	44.67	27.80	21.36	9.84	11.64
5	45	105.26	37.03	31.22	25.55	9.88	14.17
6	45	70.08	40.51	25.35	19.43	9.09	10.68
7	40	89.96	29.43	24.34	21.64	8.42	11.47
8	40	86.80	49.77	31.23	23.97	11.12	13.14
9	30	101.25	35.61	30.37	25.46	9.91	14.55
10	30	112.09	41.38	35.04	28.89	11.92	16.46
11	20	138.47	43.92	31.65	35.05	16.05	16.74
12	20	162.05	54.18	43.34	41.58	17.72	22.07
13	20	118.44	31.91	10.68	28.92	15.23	10.28
14	20	149.68	50.57	41.22	38.49	16.17	20.91
15	20	89.79	25.78	9.90	22.03	13.39	8.00
16	20	104.41	44.69	10.80	22.04	19.26	9.07
17	20	124.87	37.53	23.61	30.84	15.42	13.27
18	10	79.57	29.42	25.48	21.98	9.31	13.16
19	10	96.02	36.51	31.16	26.68	11.63	15.92
20	10	121.95	46.16	39.50	33.86	14.69	20.19
21	10	137.82	54.91	46.36	36.37	14.76	20.14
22	0	107.53	55.18	40.24	26.71	16.07	12.25
23	0	76.43	30.93	27.04	22.58	10.47	13.27
24	0	115.96	50.59	40.71	34.55	16.11	20.62
25	0	98.08	39.94	34.69	28.93	13.43	17.06
26	0	68.60	27.53	24.21	20.28	9.34	11.91

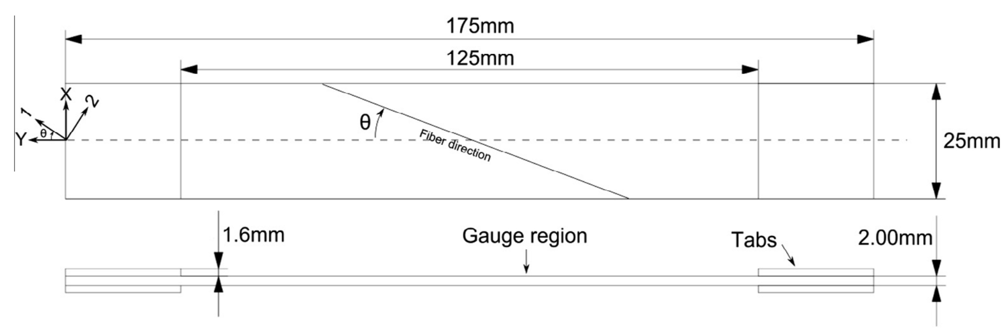

Fig. 10. Unidirectional off-axis tension specimen.

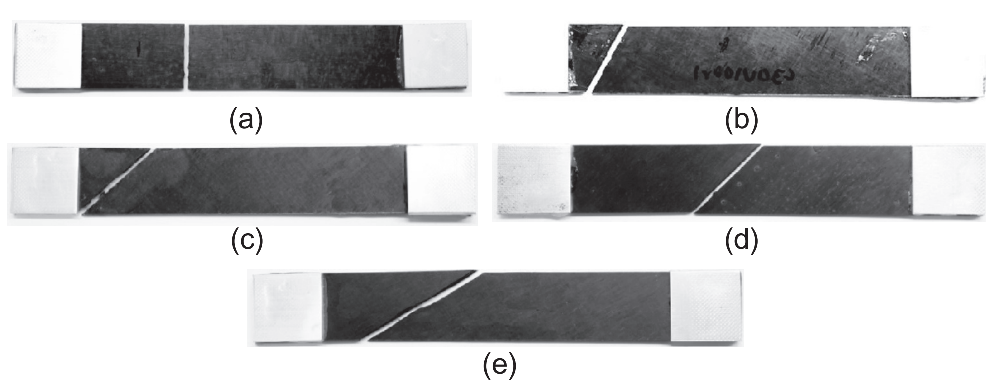

Fig. 11. Failed off-axis tension specimen. Fibre angle: (a) 90°, (b) 60°, (c) 50°, (d) 45°, (e) 30°.

4.2. Processed results

As the neat resin specimen is composed of one material which is isotropic (EP280 resin); micromechanical analysis was not required. Instead the specimen was modelled in FEMAP v10.0.2 where the forces at failure in the x and y directions were applied to the specimen similar to that described in Section 2.3 and a previous investigation by the authors [21,38]. The principal stresses at the centre node of the gauge region were extracted and recorded as the stresses at failure. These stresses are shown in Table 6. From FEA it was found that the out-of-plane stresses were one hundredth in order of magnitude of the in-plane stress values. Thus in Table 6, the value of σ_3 is assumed to be equal to zero for all the tests.

Table 5
Critical principal stresses & forces at failure obtained in the matrix for uniaxial tension tests. (Stresses have been averaged based on the four fibre configurations examined; their standard deviations are shown.)

Test Nº	Fibre angle (°)	Failure force (N)	σ_1 (MPa)	σ_2 (MPa)	σ_3 (MPa)	Standard deviation σ_1 (MPa)	Standard deviation σ_2 (MPa)	Standard deviation σ_3 (MPa)
1	90	2380	89.94	37.34	35.55	31.15	13.02	12.29
2	90	2441	92.35	38.34	36.43	31.94	13.35	12.57
3	90	2113	82.03	34.04	32.49	25.92	10.86	10.31
4	90	2408	90.95	37.76	35.96	31.42	13.14	12.40
5	60	2558	107.62	28.29	−6.03	28.03	9.77	8.71
6	60	2513	105.78	27.83	−5.87	27.56	9.62	8.59
7	50	2427	112.70	20.49	−38.81	47.52	7.36	22.05
8	45	3615	118.53	26.09	−24.25	29.49	8.99	14.17
9	45	3689	126.21	26.53	−30.30	30.01	9.16	7.66
10	45	3349	114.61	24.09	−27.53	27.24	8.31	6.95
11	45	3157	108.12	22.75	−25.92	25.78	7.86	6.55
12	40	3622	111.53	22.64	−29.13	21.93	6.13	9.08
13	30	5977	121.99	20.16	−47.56	26.87	6.92	7.56
14	30	5518	112.74	18.67	−43.84	24.87	6.42	7.03

Table 6
Critical principal stresses & forces obtained at failure in the neat resin under biaxial and uniaxial tension tests.

Test Nº	Failure force in the X direction (N)	Failure force in the Y direction (N)	σ_1 (MPa)	σ_2 (MPa)	σ_3 (MPa)
1	6053	0	133.13	−43.55	0.00
2	4730	6245	103.32	59.07	0.00
3	6366	4852	105.08	60.90	0.00
4	5756	5110	89.82	70.96	0.00
5	5607	4516	90.82	58.98	0.00
6	6232	3019	115.33	21.57	0.00
7	0	5548	122.02	−39.94	0.00
8	2023	N/A (Uniaxial)	146.00	0.00	0.00
9	1636	N/A (Uniaxial)	155.00	0.00	0.00
10	1785	N/A (Uniaxial)	149.00	0.00	0.00

5. Discussion

The three different experiments are compared to observe similarities in the stresses obtained upon matrix failure. Seven comparisons are made as discussed below.

(1) Compare the results for the fibre reinforced biaxial specimen with von-Mises failure criterion.
(2) Compare the results for the fibre reinforced biaxial specimen with the 1st Stress Invariant.
(3) Compare the results for the off-axis fibre reinforced uniaxial specimen with von-Mises failure criterion.
(4) Compare the results for the off-axis fibre reinforced uniaxial specimen with the 1st Stress Invariant.
(5) Compare the results for the neat resin biaxial specimen with von-Mises failure criterion.
(6) Compare the results for the neat resin biaxial specimen with the 1st Stress Invariant.
(7) Compare the 1st Stress Invariant for the three different experiments.

Fig. 12 clarifies what the different failure criterions discussed in this paper look like when drawn in 3D stress space. The results from the comparisons are summarised in Table 7 below.

For discussion purposes examining comparison 1 and 2; Tests 11–17, 18–21 and 22–26 represent the 20°, 10° and 0° biaxial FRPC tests respectively. This is shown in Table 7 as the average of the results in order to overcome the scatter experienced in those particular fibre angles tested. The reader can refer to Table 4 for the full set of data.

The general equations for von-Mises and the 1st Stress Invariant is given by Eqs. (4) and (5).

$$\sigma_{vm} = \left\{0.5\left[(\sigma_1-\sigma_2)^2+(\sigma_1-\sigma_3)^2+(\sigma_2-\sigma_3)^2\right]\right\}^{0.5} \tag{4}$$

$$J_1 = \sigma_1+\sigma_2+\sigma_3 \tag{5}$$

where:

σ_1, σ_2, and σ_3 are the three principal stresses (max, mid, and min respectively).
σ_{vm} is the von-Mises stress.
J_1 is the 1st Stress Invariant and failure is predicted when J_1 is equal to a critical value termed X_t.

RSS was calculated using Eq. (6). Here y_i is the experiment value and $f(x_i)$ is the predicted value.

$$RSS = \sum_{i=1}^{n}(y_i - f(x_i))^2 \tag{6}$$

5.1. Comparisons 1 and 2

Comparison 1 compares the matrix failure results with von-Mises failure criterion (Eq. (4)). A least squares linear regression using Eq. (6) was performed. The values of σ_1, σ_2, and σ_3 are known from Table 4. This implies that σ_{vm} is the only unknown in the von-Mises failure criterion given by Eq. (4). Thus various values of σ_{vm} are estimated and the RSS value given by Eq. (6) was recorded. The value of σ_{vm} which gave the lowest RSS was chosen as giving the best fit to the matrix failure results. The obtained von-Mises failure criterion using this approach is given by Eq. (7) and plotted as 'regression 1' in Fig. 13.

In comparison 2, the matrix failure results are compared against the 1st Stress Invariant which is proposed in Onset theory [8,9] to predict dilatational (tensile) failure of the matrix. The relationship for the 1st Stress Invariant (Eq. (5)) was obtained using the same approach discussed for the von-Mises failure criterion. Here J_1 is the one unknown parameter and thus different values of J_1 were estimated and the value that gave the lowest RSS value was chosen. This value was 167.5 MPa given by Eq. (8).

Due to the nature of the biaxial specimen design presented it is difficult to obtain a pure uniaxial matrix failure point, especially since the results are processed using micromechanical analysis involving RVEs. For demonstration purposes as von-Mises is typically based on uniaxial test data in order to determine the value of σ_{vm}, the authors use the value of 167.5 MPa obtained from Eq. (8) to come up with the relationship given by Eq. (9) and plotted on Fig. 13 as 'regression 2'.

$$\left\{0.5\left[(\sigma_1-\sigma_2)^2+(\sigma_1-\sigma_3)^2+(\sigma_2-\sigma_3)^2\right]\right\}^{0.5} = 78.5 \tag{7}$$

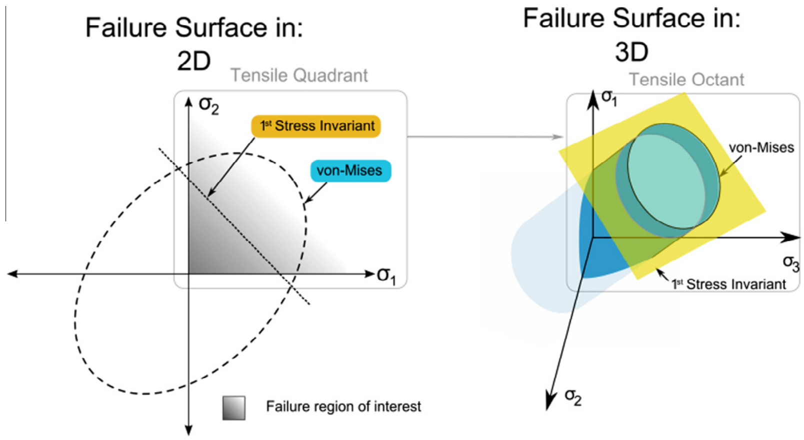

Fig. 12. 2D and 3D representations of failure criteria in the tensile quadrant/octant.

Table 7
Comparison of experimental results with von-Mises failure criterion and the 1st Stress Invariant.

Test N°	% Difference between experimental data and failure prediction found in comparison:					
	1	2	3	4	5	6
1	13.13	4.39	78.01	35.24	–	–
2	110.32	7.53	74.29	38.80	21.66	6.00
3	33.30	−9.97	91.53	23.38	19.70	8.35
4	131.53	−11.03	75.42	36.76	27.19	4.95
5	99.21	3.59	1.80	7.88	32.36	−2.22
6	139.75	−18.84	0.68	6.10	18.11	−10.64
7	97.48	−14.19	21.85	−21.61	–	–
8	130.93	0.18	17.80	−0.03	2.62	−4.70
9	85.42	−0.16	23.26	1.70	6.50	1.17
10	73.51	12.55	17.63	−7.67	3.65	−2.74
11			14.01	−12.83		
12			17.14	−12.76		
13	39.13 (avg. T11-T17)	14.92 (avg. T11-T17)	28.05	−21.44		
14			23.82	−27.26		
15						
16						
17						
18–21 (avg.)	80.84	11.17				
22–26 (avg.)	113.98	0.02				
Residual sum of squared errors (RSS):	127,716	3,848	20,598	12,990	20,575	655

$$\sigma_1 + \sigma_2 + \sigma_3 = 167.5 \tag{8}$$

$$\left\{0.5\left[(\sigma_1 - \sigma_2)^2 + (\sigma_1 - \sigma_3)^2 + (\sigma_2 - \sigma_3)^2\right]\right\}^{0.5} = 167.5 \tag{9}$$

From Table 7 it is seen that the errors predicted by the 1st Stress Invariant failure criterion are fairly low, with an average error of 8%. Whilst for the von-Mises failure criterion given by Eq. (7) the difference between the model prediction and matrix failure results are very high, with an average error of 88%. The poor fit is also reflected in the residual sum of squared error (RSS) which is 33 times greater than that obtained when using the 1st Stress Invariant.

5.2. Comparisons 3 and 4

Comparison 3 and 4 uses the processed data obtained for matrix failure in the off-axis uniaxial specimens. The experimental results are compared against von-Mises failure criterion and the 1st Stress Invariant. The equations for the two von-Mises regressions (Eqs. (10) and (12)) and the 1st Stress Invariant (Eq. (11)) were obtained using the same process discussed in Section 5.1. If we interpret the values obtained from the regression; in Eq. (10) a uniaxial intercept point (or failure stress) of 104.0 MPa is found that fits the results the best whilst for the 1st Stress Invariant a much higher uniaxial tensile stress of 120.4 MPa is predicted for failure.

From Table 7 it can be seen that von-Mises failure criterion over predicts matrix failure for all the experimental results, whilst the 1st Stress Invariant does a much better job in explaining the materials failure. In the case of 'Regression 1' (Eq. (10)) where von-Mises is regressed on all the test data, it can be seen from Fig. 14 that the failure criterion does a poor job in predicting material failure. This is also confirmed by the RSS value which is about double that obtained for the 1st Stress Invariant failure criterion.

$$\left\{0.5\left[(\sigma_1 - \sigma_2)^2 + (\sigma_1 - \sigma_3)^2 + (\sigma_2 - \sigma_3)^2\right]\right\}^{0.5} = 104.0 \tag{10}$$

$$\sigma_1 + \sigma_2 + \sigma_3 = 120.4 \tag{11}$$

$$\left\{0.5\left[(\sigma_1 - \sigma_2)^2 + (\sigma_1 - \sigma_3)^2 + (\sigma_2 - \sigma_3)^2\right]\right\}^{0.5} = 120.4 \tag{12}$$

Note that the 1st Stress Invariant for this type of specimen is found to over predict failure for the 90–60° off-axis specimens (tests 1–6), whilst under predicting failure for the 50–30° specimens (tests 7–14). The authors are not interested in presenting a new failure criterion in this paper, but simply present the experimental results with the intention of comparing it against two exist-

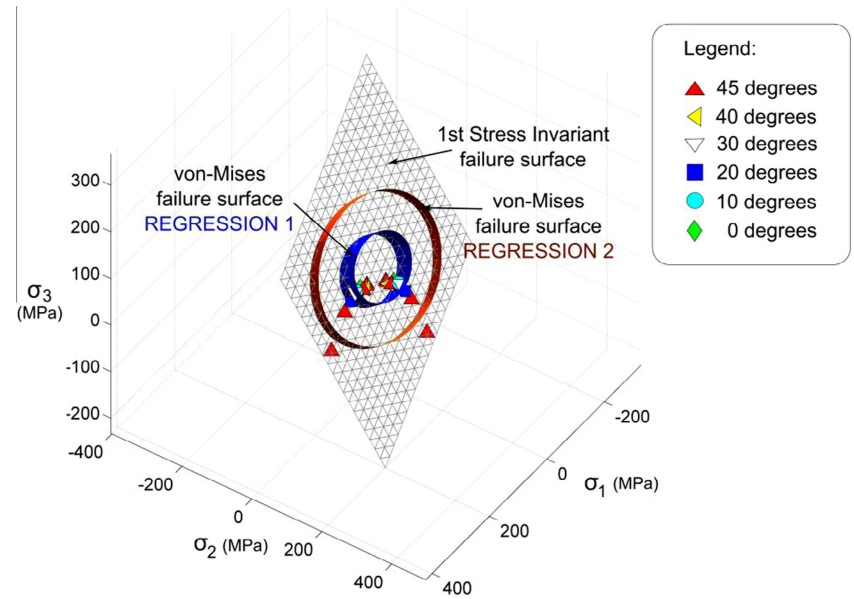

Fig. 13. 3D plot of biaxial FRPC results with the 1st Stress Invariant and von-Mises failure surfaces. 'Regression1': von-Mises based on uniaxial data, Eq. (7). 'Regression 2': von-Mises based on biaxial data, Eq. (8).

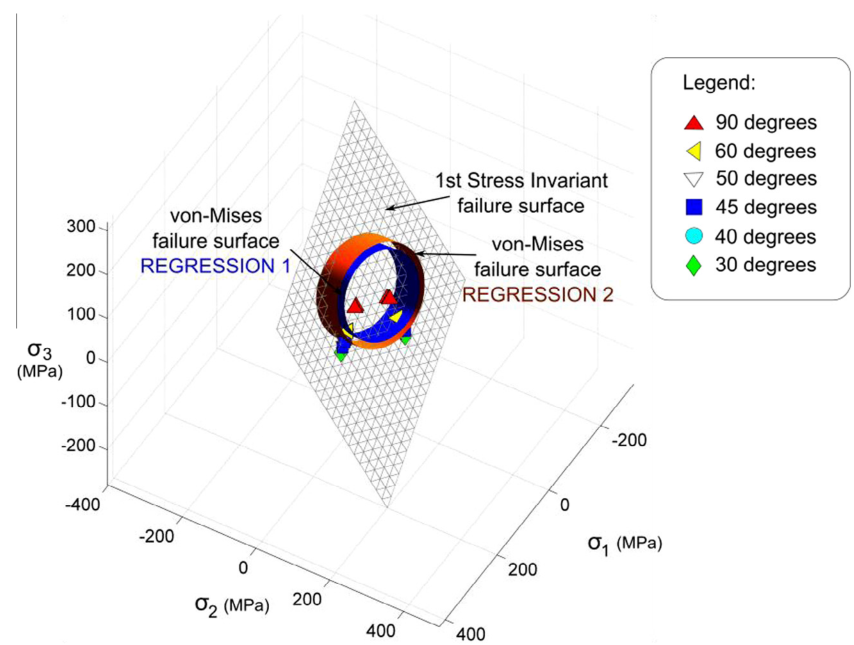

Fig. 14. 3D plot of off-axis UD experimental results with the 1st Stress Invariant and von-Mises failure surfaces. 'Regression1': von-Mises based on uniaxial data, Eq. (10). 'Regression 2': von-Mises based on biaxial data, Eq. (11).

ing failure criterions. However, it can be noted that if a second curve fitting parameter termed 'K' is introduced to the σ_3 variable, a much better fit is obtained (when $K = 0.15$). This is given by Eq. (13).

$$\sigma_1 + \sigma_2 + K\sigma_3 = J_1 \tag{13}$$

This modified model will not be looked into further in this paper as the primary focus is on the biaxial FRPC specimen, which demonstrates a good fit with the standard form of the 1st Stress Invariant. A possible cause to this slight change in the model may be attributed to the specimen design which suffers from large amounts of shear and stress concentrations at the clamping regions of the specimen as discussed by several authors in literature [14,15,19].

5.3. Comparison 5 and 6

The final type of specimen tested is made up of the neat resin material which makes up the matrix constituent in the previous two specimen designs tested. These experimental results are also compared against von-Mises failure criterion and the 1st Stress Invariant. A plot of the experimental points along with these two failure criteria is shown in Fig. 15.

A least squares regression analysis similar to the one discussed in Section 5.1 was performed using the tensile results. Eqs. (14) and (16) are obtained for von-Mises whilst the 1st Stress Invariant is given by Eq. (16). If we interpret the values obtained from the regression; in Eq. (14) a uniaxial intercept point (or failure stress) of 112.4 MPa was found that fits the results the best whilst for the

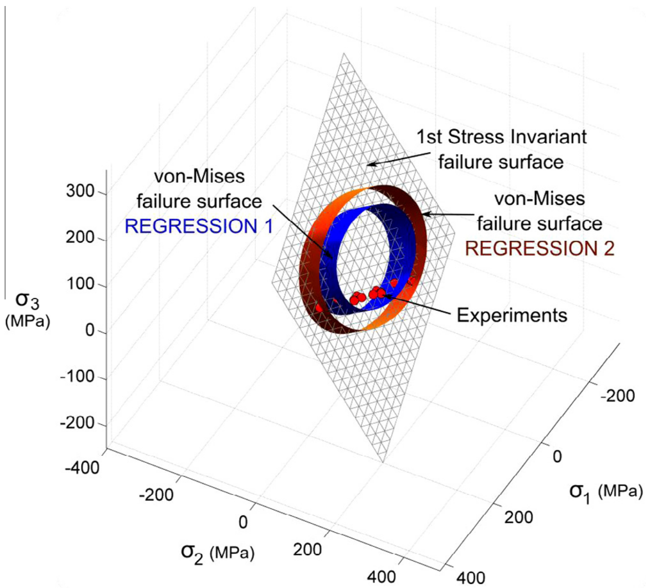

Fig. 15. 3D plot of neat resin experimental results with the 1st Stress Invariant and von-Mises failure surfaces. 'Regression1': von-Mises based on uniaxial data, Eq. (14). 'Regression 2': von-Mises based on biaxial data, Eq. (15).

1st Stress Invariant (Eq. (15)) a much higher uniaxial tensile stress of 153.2 MPa is predicted for failure.

$$\left\{0.5[(\sigma_1-\sigma_2)^2+(\sigma_1-\sigma_3)^2+(\sigma_2-\sigma_3)^2]\right\}^{0.5}=112.4 \tag{14}$$

$$\sigma_1+\sigma_2+\sigma_3=153.2 \tag{15}$$

$$\left\{0.5[(\sigma_1-\sigma_2)^2+(\sigma_1-\sigma_3)^2+(\sigma_2-\sigma_3)^2]\right\}^{0.5}=153.2 \tag{16}$$

Looking at Table 7, the linear fit using the 1st Stress Invariant was found to give the best prediction of failure in the material, with an average error prediction of 13%. This is also confirmed when the RSS value is observed. Here the goodness of fit was 30 times better for the 1st Stress Invariant compared to the prediction of matrix failure given by von-Mises.

5.4. Overall comparison/comparison 7

In all three experiments performed, von-Mises failure criterion severely over predicted matrix failure. As all the experimental points tend to cluster on the inside of the von-Mises failure surface, a good match was found using the 1st Stress Invariant which is a flat plane when drawn in 3D. The 1st Stress Invariant was much better in predicting matrix failure. Hence, the experimental results suggest that there is a truncation in the tensile quadrant of the materials failure envelope.

A plot of the suggested failure envelope in the tensile quadrant for matrix failure is shown in Fig. 16. Although all three sets of experiments exhibit a close correlation to the 1st Stress Invariant, they do have different magnitudes. Eq. (17) summarises these differences. The baseline experiment is considered to be the biaxial FRPC experiments as this specimen design includes the presence of fibres whilst improving on the off-axis tests. The off-axis fibre reinforced specimens were found to have the lowest stresses at failure, and this may be attributed to the inherent downfall of the specimen design suffering from large shear stresses in the clamping locations. This was also noted by others in literature [14,15,19]. Despite this, the results still show a similar trend as the biaxial fibre reinforced specimens, where a truncation exists in this tensile quadrant. The biaxial tests performed on the neat resin specimens were found to fail at slightly lower stress values (by 8%) compared to the biaxial fibre reinforced specimens. The experiment results still demonstrated a truncation in the tensile quadrant. Although this difference is very minor it may be explained by the findings of others which state that the in-situ flow stress behaviour of the epoxy matrix can be different to that obtained from mechanical tests of matrix coupons due to the differences in the curing process with and without the presence of fibres [37,39,40]. Further investigation into this behaviour is outside the scope of this paper, but has been investigated by others [37,39,40].

$$X_t^{BFR}=1.09X_t^{NEAT}=1.39X_t^{UFR} \tag{17}$$

where:

X_t^{BFR} is the critical stress value given by the 1st Stress Invariant for the biaxial fibre reinforced specimen given by J_1 in Eq. (8).
X_t^{NEAT} is the critical stress value given by the 1st Stress Invariant for the biaxial neat resin specimen given by J_1 in Eq. (15).

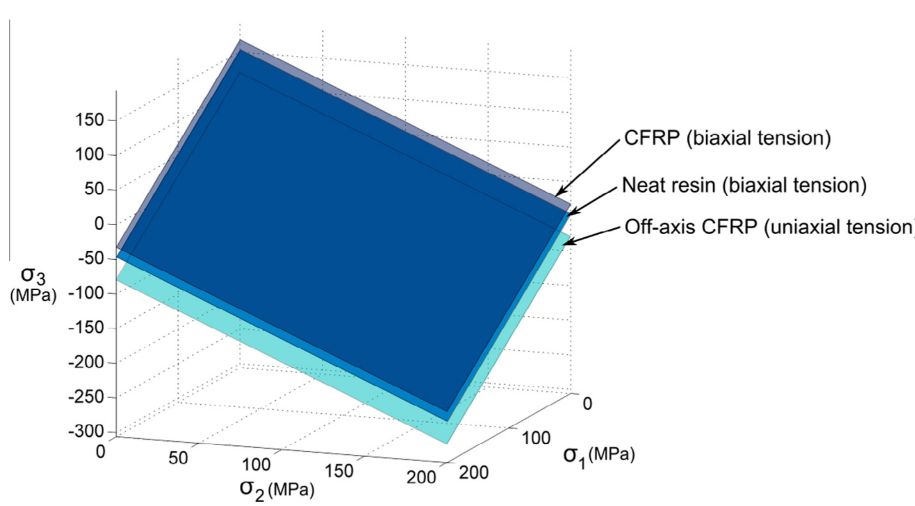

Fig. 16. Plot of matrix failure planes given by the 1st Stress Invariant for the three different experiments discussed in this paper.

X_t^{UFR} is the critical stress value given by the 1st Stress Invariant for the uniaxial fibre reinforced specimen given by J_1 in Eq. (11).

6. Conclusions

The presented fibre reinforced biaxial specimen was found to successfully demonstrate matrix failure originating within the gauge region. Through performing several tests under different loading ratios, the tensile quadrant of a stress based failure envelope was populated. A superimposing technique utilising micromechanical analysis was presented by the authors to extract the stresses on the matrix at failure. In total, three sets of experiments were performed with all demonstrating a similar trend. Overall, the fibre reinforced biaxial tests were found to demonstrate a good match with the 1st Stress Invariant with an average model prediction error of 8%.

References

[1] Jeffry W, Mayes S, Christopher K, Richard M. Comparison of MCT failure prediction techniques and experimental verification for biaxially loaded glass fabric-reinforced composite laminates. J Compos Mater 2004;38:2165–81.

[2] Reddy JN. Mechanics of laminated composite plates. CRC Press; 1997.

[3] Helius: MCT Technical Manual. Version 1.0 ed 2009: Firehole Technologies.

[4] Welsh JS. Comparison of MCT failure prediction techniques and experimental verification for biaxially loaded glass fabric-reinforced composite laminates. J Compos Mater 2004;38:2165–81.

[5] Shokrieh MM, Lessard LB. Progressive fatigue damage modelling of composite materials, Part II: material characterization and model verification. J Compos Mater 2000;34:1081–116.

[6] Chi SL, Jeong HK, Seul KK, Dong MR, Jae ML. Initial and progressive failure analyses for composite laminates using puck failure criterion and damage-coupled finite element method. Compos Struct 2015;121:406–19.

[7] Ana C, Toby M, Kent H. Finite element guidelines for simulation of fibre-tension dominated failures in composite materials validated by case studies. Compos Struct 2015;126:299–313.

[8] Hart-Smith LJ. Application of the strain invariant failure theory (SIFT) to metals and fibre-polymer composites. Philos Mag 2010;90:4263–331.

[9] Gosse JH, Christensen S. Strain invariant failure criteria for polymers in composite materials. In: AIAA Structural Dynamics, and Materials Conference, 2001. p. 45–55.

[10] Kyo J, Yuanchen H, Young L, Ha SK. Distribution of micro stresses and interfacial tractions in unidirectional composites. J Compos Mater 2008;42:1825–49.

[11] Asp L, Berglund A, Talreja R. A criterion for crack initiation in glassy polymers subjected to a composite-like stress state. Compos Sci Technol 1996;56:1291–301.

[12] Pipes RB, Gosse JH. An onset theory for irreversible deformation in composite materials. In: Proceedings of 17th International Conference on Composite Materials (ICCM 17), Edinburgh, 27–31 July 2009.

[13] Pierron F, Alloba E, Surrel Y, Vautrin A. Whole-filed assessment of the effects of boundary conditions on the strain field in off-axis tensile testing of unidirectional composites. Compos Sci Technol 1998;58:1939–47.

[14] Sun CT, Chung I. An oblique end-tab design for testing off-axis composite specimens. Composites 1993;24:619–23.

[15] Xiao Y, Kawai M, Hatta H. An integrated method for off-axis tension and compression testing of unidirectional composites. J Compos Mater 2010;46:657–69.

[16] Quek SC, Waas AM, Shahwan KW, Agaram V. Compressive response and failure of braided textile composites: Part 1-experiments. Int J Non-Linear Mech 2004;39:635–48.

[17] Serna Moreno MC, Lopez Cela JJ. Failure envelope under biaxial tensile loading for chopped glass-reinforced polyester composites. Compos Sci Technol 2011;72:91–6.

[18] Serna Moreno MC, Curiel-Sosa JL, Navarro-Zafra J, Martinez Vicente JL, Lopez Cela JJ. Crack propagation in a chopped glass-reinforced composite under biaxial testing by means of XFEM. Compos Struct 2015;119:264–71.

[19] David AE, Diego C, Hugo E, Ricardo R, Oliver P. Biaxial tensile strength characterization of textile composite materials. In: Composites and their properties. InTech; 2012. http://dx.doi.org/10.5772/48105.

[20] Chowdhury N, Chiu WK, Wang J. Biaxial specimen design for structures subjected to muli-axial loads. Adv Mater Res 2014;891:1633–8.

[21] Chowdhury N, Chiu WK, Wang J, Yan W. Comparison of failure criteria examining matrix dominant failure under biaxial loading. In: ACAM 8, 8th Australasian congress on applied mechanics, 2014.

[22] GMS Composites, <http://www.gmscomposites.com/prepreg-range/>.

[23] Chowdhury NT, Chiu WK, Wang J. Design of a flat plate specimen suitable for biaxial tensile tests on polymer materials. Polym Polym Compos, 23(9), in press.

[24] Li W, Cai H, Li C, Wang K, Fang L. Micro-mechanics of failure for fatigue strength prediction of bolted joint structures of carbon reinforced polymer composites. Compos Struct 2015;124:345–56.

[25] ASTM D3039. Standard test method for tensile properties of polymer matrix composites. West Conshohocken, PA: ASTM International; 2000.

[26] ASTM D5379. Standard test method for shear properties of composite materials by the V-notched beam method. West Conshohocken, PA: ASTM International; 2012.

[27] Kaw. Mechanics of composite materials. 2nd ed. CRC Press; 2006.

[28] FEMAP v10.0.2 64-bit. Finite Element Analysis software package.

[29] Lane C. Acoustic wave propagation in anisotropic media, Part 2. Switzerland: Springer International Publishing; 2014.

[30] Pagano NJ, Halpin JC. Influence of end constraint in the testing of anisotropic bodies. J Compos Mater 1968;2:18.

[31] Meremonti P, Russo R. On the Von Mises-Sternberg version of Saint-Venant's principle in plane linear elastostatics. Arch Ration Mech Anal 1994;128:207–21.

[32] ABAQUS CAE 6.13 Standard edition. Finite element analysis software package.

[33] Szekrenyes A, Jozsef U. Finite element modelling of the damage and failure in fibre reinforced composites (overview). Periodica Polytechnica Ser Mech Eng 2002;46:139–58.

[34] Xia Z, Chen Y, Ellyin F. A meso/micro-mechanical model for damage progression in glass-fibre/epoxy cross-ply laminates by finite-element analysis. Compos Sci Technol 2000;60:1171–9.

[35] Tsai SW. Residual stress and strains, composite design. In: Tsai SW, editor. 4th ed. Think Composites; 1988.

[36] Chowdhury NT, Chiu WK, Wang J, Yan W. Residual stresses introduced to composite structures due to the cure regime. In: Proceedings under review in the 7th Asia pacific international symposium on aerospace technologies (APISAT 2015), Australia: 25–27 November 2015.

[37] Lee S, Munro M, Scott RF. Evaluation of three in-plane shear test methods for advanced composite materials. Composites 1990;21:495–501.

[38] Steve L. Characterization and failure analysis of plastics. ASM International; 2003. p. 99.

[39] Essam T, Carlos G, Javier L, Molina-Aldareguia JM. Mechanics of shear deformation in fiber-reinforced polymers: experiments and simulation. Int J Fract 2009;158:197–209.

[40] Yerramalli CS, Waas AM. In situ matrix shear response using torsional test data of fiber reinforced polymer composites. J Eng Mater Technol 2002;124:152–9.